Journal of Zhejiang University-SCIENCE B (Biomedicine & Biotechnology) *2022 23(9):784-790*
www.jzus.zju.edu.cn; www.springer.com/journal/11585
E-mail: jzus_b@zju.edu.cn

Correspondence

https://doi.org/10.1631/jzus.B2200107

Use of folic acid nanosensors with excellent photostability for hybrid imaging

Denis KUZNETSOV[1,4]✉, Sergey DEZHUROV[2], Dmitri KRYLSKY[2], Valery NOVIKOV[3], Valery NESCHISLIAEV[4], Anastasiia KUZNETSOVA[5]

[1]*G.N. Gabrichevsky Scientific and Research Institute of Epidemiology and Microbiology, Moscow 125212, Russia*
[2]*Research Institute of Applied Acoustics, Center of High Technologies, Dubna 141980, Russia*
[3]*Perm State Medical University, Perm 614000, Russia*
[4]*Perm State Pharmaceutical Academy, Perm 614990, Russia*
[5]*Perm State Humanitarian Pedagogical University, Perm 614990, Russia*

Sentinel lymph node (SLN) mapping and tumor-boundary delineation play a key role in cancer surgery, as they have great potential to reduce surgical intervention and increase relapse-free survival rates of patients. The autofluorescence imaging (AFI) method can improve the efficiency of tumor delineation and optimize the scope of surgical intervention, but there are still no fluorescent drugs that can be used with such a method to form a hybrid imaging technique. Another problem is bleaching when fluorescent dyes are conjugated with folic acid. This study reports, for the first time, nanosensors with excellent photostability and compatibility with endoscopes for AFI, which makes simultaneous hybrid imaging possible. After functionalization of the quantum dot (QD) surfaces, we found that they bound effectively to MCF-7 cancer cells. The diagnostic value of simultaneous hybrid imaging using common AFI equipment in delineating tumor boundaries and mapping SLN can reduce the cost of diagnosis and increase its reliability.

Stomach cancer is one of the most common types of cancer in the world, accounting for more than one million cases per year and 5.7% of all cancer diagnoses (van Cutsem et al., 2016; Bray et al., 2018; Sung et al., 2021). Generally, its prognosis is unfavorable, as evidenced by the five-year survival rate and the fact that when diagnosed, most cases already have metastases (Rawla and Barsouk, 2019). The main method of treatment is surgical intervention. The most adequate degree of lymph node dissection during stomach cancer surgery is highly debatable among doctors and researchers because there are still no reliable intraoperative methods to identify affected lymph nodes. D1 gastrectomy or subtotal resection of the stomach with lymph dissection remains the standard operating intervention in most clinics, with D2 and D3 lymphadenectomies being considered extended. To date, there are no clear medical indications as to the extent and adequacy of performing extended intra-abdominal lymph dissection in the case of resectable stomach cancer. Several surgeons have argued in favor of extended (D2) lymphadenectomy, as it would provide better local-regional control of the disease. However, increased morbidity and mortality initially attributed to D2 lymphadenectomy, and the fact that there were no survival benefits registered, made Western surgeons reconsider surgical intervention tactics and turn their attention to a more limited D1 lymphadenectomy (Bonenkamp et al., 1999; Cuschieri et al., 1999; Degiuli et al., 2010).

Nevertheless, a long-term (15-year) follow-up carried out by Dutch researchers changed the overall picture, as it reported a significant decrease in the frequency of relapses after the D2 procedure. D2 lymphadenectomy is currently recommended for all patients suffering resectable advanced stomach cancer (Cummings et al., 2021). Since gastrectomy with D2 lymph dissection involves a high level of surgical

✉ Denis KUZNETSOV, denis.pfa@gmail.com
Denis KUZNETSOV, https://orcid.org/0000-0003-0884-848X

Received Mar. 3, 2022; Revision accepted May 22, 2022;
Crosschecked July 12, 2022

intervention, relatively high morbidity and mortality rates are to be expected, even though it is performed in highly specialized medical centers (Songun et al., 2010).

To determine the extent of the malignant process and completely excise the primary tumor on the stomach wall within healthy tissue, it is recommended to use equipment that improves the efficiency of tumor-boundary detection by AFI (Pantalone et al., 2007; Tada et al., 2011). In addition, recent clinical studies have shown that image enhancement using AFI is advantageous for laparoscopic intraoperative diagnosis of serous invasion and peritoneal dissemination in the case of advanced gastric cancer. It also provides a significantly higher frequency of complete resection in early stomach cancer (Ahn et al., 2011; Matsui et al., 2021).

Use of fluorescent dyes for SLN mapping, together with AFI, can increase the effectiveness of diagnostics. Some specialists have been trying to optimize surgical tactics by mapping SLNs with various chemical dyes. One of the first means for mapping was non-specific dyes. Initially, this involved a mucous-membrane injection of methylene blue, after which indocyanine green (ICG), a fluorescent dye, came into use. This agent was more sensitive than chromogenic dyes. Among the available imaging methods, only fluorescence imaging (FI) provides real-time images with millimeter resolution, and this is the reason why it has aroused interest among surgeons considering intraoperative FI (Hokimoto et al., 2018; Kim et al., 2019; Jung et al., 2021). Results of a meta-analysis of 13 clinical trials involving 971 patients have demonstrated that detection of SLNs by near-infrared or FI using FI ICG is technically feasible (He et al., 2018). However, one of the main constraining factors for the introduction of fluorescent mapping of lymph nodes is the high cost of diagnostic equipment and organic dye (ICG), as well as potential low specificity and false-positive results due to the effects of tissue perfusion. A promising way to solve these problems is to develop a nanosensor that will bind specifically to cancer cells and at the same time be compatible with endoscopes having an AFI mode. This combination will provide simultaneous hybrid imaging without the need to develop special equipment.

Folic acid is an important substance in human metabolism and is involved in nucleotide base synthesis; its derivatives have been used for targeted treatment and imaging of tumor tissues since the 1990s. Folic acid has several receptors that ensure its transfer through the cell wall. The most common one is folate receptor-α (FR-α), which is overexpressed in malignant ovary, stomach, colon, and breast tissues (Hashemzadeh et al., 2021; Sakai et al., 2021). Various conjugates related to folic acid and its derivatives have been developed (Liang et al., 2019; Augustine et al., 2021; Shakeri-Zadeh et al., 2021; Skripka et al., 2021), one of which is folate-fluorescein isothiocyanate (FITC) (van Dam et al., 2011). However, FITC emits green fluorescence (about 520 nm) and is not suitable for deep-tissue imaging. For this purpose, dyes emitting in the near-infrared region (650–900 nm) are most suitable, since their penetration into tissues is high and their autofluorescence is low, which provides a high signal/background ratio (Kelderhouse et al., 2013; Potara et al., 2021). In a study by Huang et al. (2016), a near infrared-light-absorbing carbazole-substituted BODIPY (Car-BDP) conjugate having an emission peak of 755 nm was developed with a quantum yield of 4%, which could increase to 58% when exposed to radiation at a wavelength of 710 nm. There is no data on photostability. Thus, this conjugate requires the use of non-standard and complex equipment. Photostability of the fluorescent agent is an extremely important characteristic because during a long surgery the dye may bleach, which will lead to false-negative results of intraoperative revision using FI. QDs are known to differ from common dyes by high quantum yield and high photostability. However, when they are conjugated with folic acid, the quantum yield decreases and fluorescent dyes bleach quickly as well as in case of conjugation of organic dyes with folic acid (Tung et al., 2002; Moon et al., 2003; Liu et al., 2016; Yan et al., 2016). Only recently has it been possible to achieve an increase in quantum yield and photostability, and only with graphene QDs (Zhang et al., 2019; Saljoughi et al., 2020). It has been found that suppression of nonradiative transitions by amino groups pyrolyzed from pterin plays a key role in the mechanism of high quantum yield and excellent stability. However, these studies report conjugates with a maximum absorption of 230–300 nm and fluorescence in the high autofluorescence zone of 450–550 nm, which makes them unsuitable for mapping sentinel nodes.

For these reasons, we sought to develop a fluorescent nanosensor with high photostability, low cost, specificity to cancer cells, and suitability for use with common endoscopes for AFI, which would allow for hybrid diagnostics.

This research is the first to synthesize luminescent QD conjugates within the range bordering on infrared radiation. The conjugates revealed photostability sufficient for medical applications. During conjugation with folic acid, we observed an increase in absorbance (Fig. 1a). The spectrofluorimetry data indicate that the fluorescence spectra are not shifted and their proportions do not change, but the fluorescence intensity does (Fig. 1b). The QD samples hardly changed their quantum yields when irradiated over time, which confirms their high photostability (Fig. 1c). Conjugation of QDs with folic acid resulted in a severe loss of photostability (bleaching within 30 min) and a decrease in quantum yield to 15% (Table 1). However, hydroxylation of the shell with diethanolamine led to the unexpected result of increasing the quantum yield to 31% and doubling the photostability (Fig. 1c). We believe that this surface modification led to shielding of the charge in the exciton state, which reduced the probability of its transfer to the folic acid molecule.

Microphotographs of the synthesized QDs were obtained, as well as their distribution according to size (Figs. 1d–1f). The samples had a crystalline structure. Analysis of the high-resolution images made it

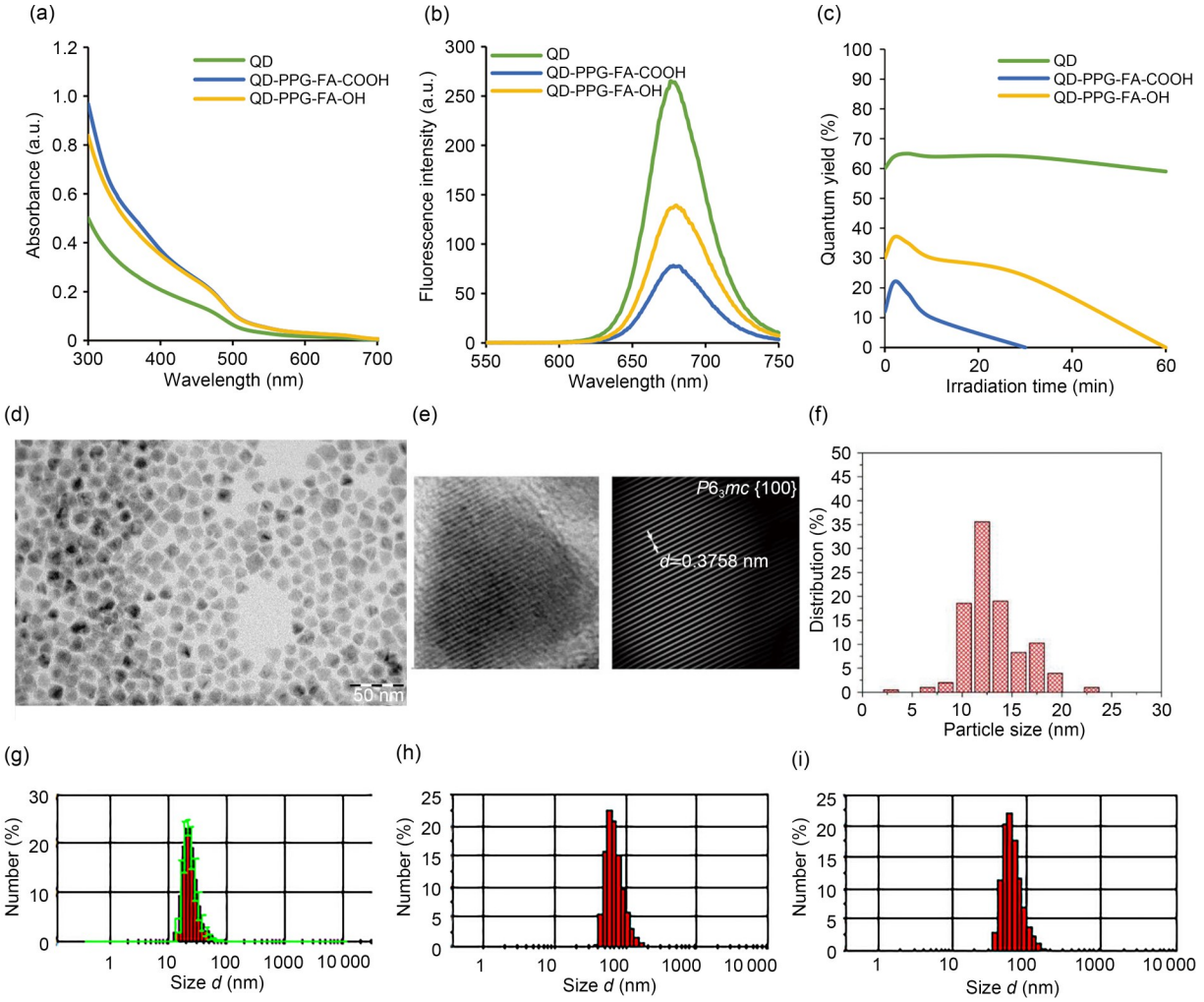

Fig. 1 Characterization of the nanoparticles. (a) Comparative spectra of conjugate absorption; (b) Comparative spectra of fluorescence; (c) Kinetics of change of fluorescence quantum yield with irradiation time; (d, e) Transmission electron microscopy (TEM) images of quantum dots (QDs); (f) Size distribution of QD; (g–i) Size distribution of hydrodynamic diameters of QD (g), QD-PPG-FA-COOH (h), and QD-PPG-FA-OH (i). a.u.: arbitrary units; PPG-FA: folic acid-conjugated polyethylenimine-modified PEGylated nanographene; COOH: carboxy; OH: oxhydryl.

possible to measure the interplanar distances (*d*) of the samples (Fig. 1e). The obtained *d* values correspond to the reported values of the $P6_3mc$ phase (Razik et al., 1990). Thus, we were able to conclude that the studied samples of synthesized nanocrystals have a hexagonal structure similar to that of wurtzite. Interestingly, most of the QDs are directed along the crystallographic direction.

We also determined the hydrodynamic diameters of the nanoparticles (Figs. 1g–1i) and found that the addition of folic acid-conjugated polyethylenimine-modified PEGylated nanographene (PPG-FA) increases the hydrodynamic diameters of the particles from 20 to 50 nm. Hydroxylation of nanoparticles has almost no effect on their size.

We evaluated the degree of binding of QD samples and conjugates to the surfaces of CHO, B16-F10, HEK-293, and MCF-7 cells, using the fluorescent signal of nanoparticles. We also found that hydroxylation unexpectedly results in increased efficiency of binding to MCF-7 cells. The highest binding occurred with MCF-7 cells (Fig. 2a). Increased binding to the membrane and accumulation of QD conjugates with folic acid in MCF-7 cells have been reported in several studies (Kumar et al., 2018; Jiao et al., 2019; Yan et al., 2020). The data from this study confirm the specificity of the interaction of folic acid with the folic acid receptor on the surface of cancer cells.

Substances chosen for concentration testing proved to be non-toxic; the software calculated half maximal inhibitory concentration (IC_{50}) values automatically. The IC_{50} values of QDs on cell lines HT29 and CHO were measured and were greater than 202.1 nmol/L. Given the low toxicity of the tested samples, IC_{50} was not determined.

To study the possibility of using the obtained QDs and their conjugates with folic acid under in vivo imaging conditions, mice were given subcutaneous and intravenous injections. We found that at the 24-h time point, when mice were injected subcutaneously, the fluorescence did not change (Fig. 2b). The pronounced fluorescent signal in the imaging of nanoparticles through the skin of the mouse confirms that nanoparticles operate in the low-autofluorescence area of tissues. This indicates the possibility of mapping the affected lymph nodes during submucosal injection of nanoparticles with minimal risk of signal loss.

Table 1 Optical characteristics of quantum dot samples and conjugates

Sample	Quantum yield (%)	Fluorescence wavelength (nm)	FWHM (nm)
QD	55	680	45
QD-PPG-FA-COOH	15	680	45
QD-PPG-FA-OH	31	680	45

COOH: carboxy; FA: folic acid; FWHM: full width at half maxima; PPG: polyethylenimine-modified PEGylated; QD: quantum dot; OH: oxhydryl.

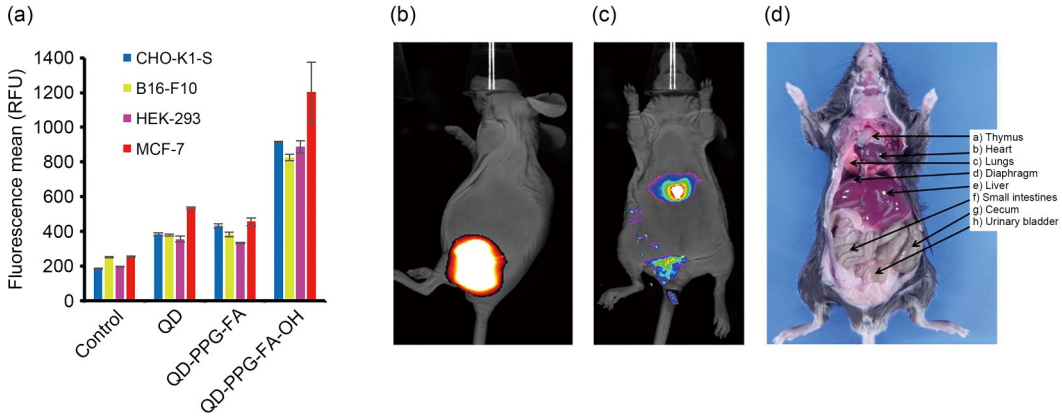

Fig. 2 Binding degrees of QD samples and conjugates to the surfaces of CHO, B16-F10, HEK-293, and MCF-7 cells. (a) Average fluorescence values of nanoparticle samples. The values are expressed as mean±SEM, *n*=4. (b–d) In vivo imaging 24 h after injection of QD-PEG-FA-OH into mice: subcutaneous (b); intravenous (c); and mouse internal organs (d). QD: quantum dot; PPG-FA: folic acid-conjugated polyethylenimine-modified PEGylated nanographene; OH: oxhydryl; RFU: relative fluorescence units; SEM: standard error of the mean.

When mice were administered intravenously, there was no evident fluorescence signal at the 24-h time point (Fig. 2c). Fluorescence was observed mainly in the liver and intestine. The hepatobiliary route of excretion of nanoparticles from the body can be explained by their size (about 50 nm). Particles larger than the pore diameter in the kidney glomeruli cannot be excreted by the renal route (Tang et al., 2016; Madajewski et al., 2018; Yang et al., 2018). Thus, we have shown that the nanosensor is retained by the tissues for a sufficient time for the operation, the fluorescent signal from the nanosensor passes through the tissues, and when it enters the bloodstream, it is quickly eliminated from the body.

To confirm the possibility of imaging a signal from a nanoparticle using common instruments for minimally invasive surgery, we used endoscopic equipment with an autofluorescence mode, produced by the company K. Storz (Tuttlingen, Germany). It has been shown that equipment in the autofluorescence mode allows effective imaging of the signal from nanoparticles (Fig. 3). Thus, the obtained nanoparticles are promising for use with endoscopes having the autofluorescence mode, which will positively affect the cost of diagnosis. In addition, it will allow the implementation of a hybrid method (tissue autofluorescence+dye fluorescence), which can increase the reliability of diagnosis. The submucosal injection pathway can be effective for preoperative mapping of lymph nodes in cancer patients. Detection of tumor dissemination pathways and identification of affected lymph nodes will allow surgeons to significantly optimize treatment tactics.

In summary, we created photostable nanosensors based on folic acid conjugates. These nanosensors have small nuclei and a hexagonal crystal structure, and are fluorescent in boundary to the near-infrared radiation range. Thus, they can be effectively used in hybrid AFI/FI. Due to their optical properties, they are highly luminescent in areas of low tissue autofluorescence, which ensures their imaging during submucosal injection and even at low dispersion concentrations (0.6 μmol/L), using conventional endoscopes. We expect hybrid imaging to significantly reduce the cost of diagnosis and increase its reliability. Given its excellent characteristics, we believe that the obtained nanosensor is a promising technique for intraoperative mapping of SLNs.

Materials and methods

Detailed methods are provided in the electronic supplementary materials of this paper.

Acknowledgments

We thank Roman IVANOV, Vice-President for Development and Research of CJSC BIOCAD (Saint Petersburg, Russia), for the opportunity to obtain flow cytofluorometry and in vivo imaging data. We are also very grateful to Alexey GRACHEV, the Head of the Laboratory of Stromal Tumor Cell Biology at the N. N. Blokhin Cancer Research Centre (Moscow, Russia), for assistance in obtaining cytotoxicity data, and to Kirill CHEREDNICHENKO, a senior researcher

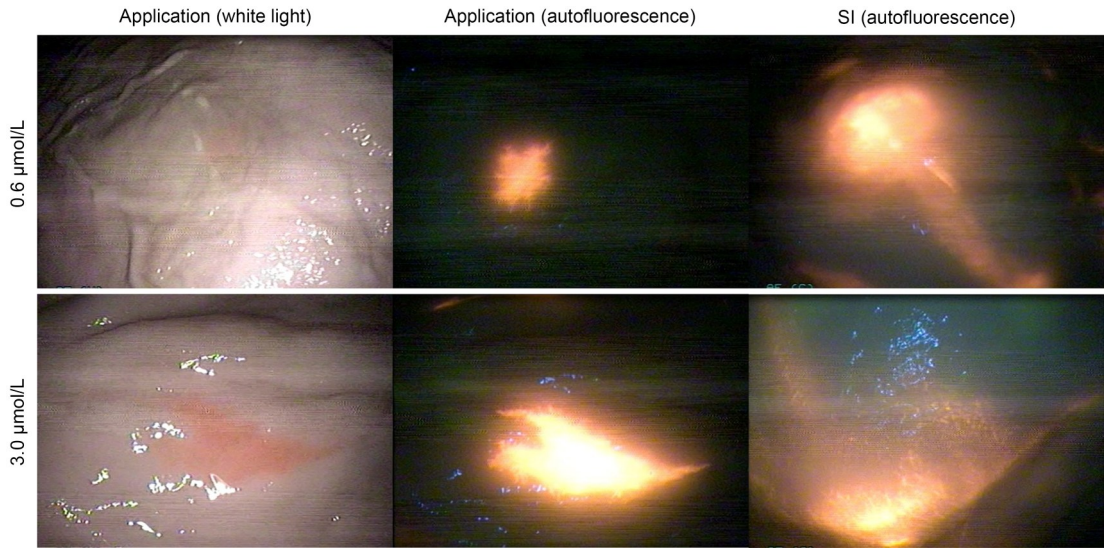

Fig. 3 Ex vivo optical imaging of nanoparticles at 0.6 and 3.0 μmol/L with application (white light), application (autofluorescence), and SI (autofluorescence) modes. SI: submucosal injection.

from Gubkin Russian State University of Oil and Gas (NRU) (Moscow, Russia), for providing transmission electron microscopy (TEM) data.

Author contributions

Denis KUZNETSOV: Conceptualization, Methodology, Data curation, Formal analysis, Project administration, Writing original draft, Visualization. Sergey DEZHUROV and Dmitri KRYLSKY: Conceptualization, Data curation, Methodology, Formal analysis, Writing review & editing. Valery NOVIKOV and Valery NESCHISLIAEV: Writing review & editing, Formal analysis. Anastasiia KUZNETSOVA: Validation, Data curation, Visualization.

Compliance with ethics guidelines

Denis KUZNETSOV, Sergey DEZHUROV, Dmitri KRYLSKY, Valery NOVIKOV, Valery NESCHISLIAEV, and Anastasiia KUZNETSOVA declare that they have no conflict of interest.

All institutional and national guidelines for the care and use of laboratory animals were followed.

References

Ahn JY, Jung HY, Choi KD, et al., 2011. Endoscopic and oncologic outcomes after endoscopic resection for early gastric cancer: 1370 cases of absolute and extended indications. *Gastrointest Endosc*, 74(3):485-493. https://doi.org/10.1016/j.gie.2011.04.038

Augustine R, Mamun AA, Hasan A, et al., 2021. Imaging cancer cells with nanostructures: prospects of nanotechnology driven non-invasive cancer diagnosis. *Adv Colloid Interface Sci*, 294:102457. https://doi.org/10.1016/j.cis.2021.102457

Bonenkamp JJ, Hermans J, Sasako M, et al., 1999. Extended lymph-node dissection for gastric cancer. *N Engl J Med*, 340(12):908-914. https://doi.org/10.1056/NEJM199903253401202

Bray F, Ferlay J, Soerjomataram I, et al., 2018. Global cancer statistics 2018: GLOBOCAN estimates of incidence and mortality worldwide for 36 cancers in 185 countries. *CA Cancer J Clin*, 68(6):394-424. https://doi.org/10.3322/caac.21492

Cummings D, Wong J, Palm R, et al., 2021. Epidemiology, diagnosis, staging and multimodal therapy of esophageal and gastric tumors. *Cancers*, 13(3):582. https://doi.org/10.3390/cancers13030582.

Cuschieri A, Weeden S, Fielding J, et al., 1999. Patient survival after D_1 and D_2 resections for gastric cancer: long-term results of the MRC randomized surgical trial. *Br J Cancer*, 79(9):1522-1530. https://doi.org/10.1038/sj.bjc.6690243

Degiuli M, Sasako M, Ponti A, 2010. Morbidity and mortality in the Italian Gastric Cancer Study Group randomized clinical trial of D1 *versus* D2 resection for gastric cancer. *Br J Surg*, 97(5):643-649. https://doi.org/10.1002/bjs.6936

Hashemzadeh A, Amerizadeh F, Asgharzadeh F, et al., 2021. Delivery of oxaliplatin to colorectal cancer cells by folate-targeted UiO-66-NH_2. *Toxicol Appl Pharmacol*, 423:115573. https://doi.org/10.1016/j.taap.2021.115573

He MF, Jiang ZW, Wang CG, et al., 2018. Diagnostic value of near-infrared or fluorescent indocyanine green guided sentinel lymph node mapping in gastric cancer: a systematic review and meta-analysis. *J Surg Oncol*, 118(8):1243-1256. https://doi.org/10.1002/jso.25285

Hokimoto N, Sugimoto T, Namikawa T, et al., 2018. A novel color fluorescence navigation system for intraoperative transcutaneous lymphatic mapping and resection of sentinel lymph nodes in breast cancer: comparison with the combination of gamma probe scanning and visible dye methods. *Oncology*, 94(2):99-106. https://doi.org/10.1159/000484050

Huang L, Li ZJ, Zhao Y, et al., 2016. Ultralow-power near infrared lamp light operable targeted organic nanoparticle photodynamic therapy. *J Am Chem Soc*, 138(44):14586-14591. https://doi.org/10.1021/jacs.6b05390

Jiao Y, Sun HY, Jia YC, et al., 2019. Functionalized fluorescent carbon nanoparticles for sensitively targeted of folate-receptor-positive cancer cells. *Microchem J*, 146:464-470. https://doi.org/10.1016/j.microc.2019.01.003

Jung MK, Cho M, Roh CK, et al., 2021. Assessment of diagnostic value of fluorescent lymphography-guided lymphadenectomy for gastric cancer. *Gastric Cancer*, 24(2):515-525. https://doi.org/10.1007/s10120-020-01121-0

Kelderhouse LE, Chelvam V, Wayua C, et al., 2013. Development of tumor-targeted near infrared probes for fluorescence guided surgery. *Bioconjugate Chem*, 24(6):1075-1080. https://doi.org/10.1021/bc400131a

Kim DW, Jeong B, Shin IH, et al., 2019. Sentinel node navigation surgery using near-infrared indocyanine green fluorescence in early gastric cancer. *Surg Endosc*, 33(4):1235-1243. https://doi.org/10.1007/s00464-018-6401-z

Kumar SSD, Mahesh A, Antoniraj MG, et al., 2018. Cellular imaging and folate receptor targeting delivery of gum kondagogu capped gold nanoparticles in cancer cells. *Int J Biol Macromol*, 109:220-230. https://doi.org/10.1016/j.ijbiomac.2017.12.069

Liang ZB, Yang YQ, Jia FJ, et al., 2019. Intrathecal delivery of folate conjugated near-infrared quantum dots for targeted in vivo imaging of gliomas in mice brains. *ACS Appl Bio Mater*, 2(4):1432-1439. https://doi.org/10.1021/acsabm.8b00629

Liu PF, Liu D, Liu YH, et al., 2016. ANTS-anchored Zn-Al-CO_3-LDH particles as fluorescent probe for sensing of folic acid. *J Solid State Chem*, 241:164-172. https://doi.org/10.1016/j.jssc.2016.06.014

Madajewski B, Chen F, Ma K, et al., 2018. Dual modality imaging of melanoma using clinically-translated ultrasmall silica nanoparticles targeting integrin and melanocortin-1 receptor expressing melanoma models. *J Nucl Med*,

59(S1):196.

Matsui R, Inaki N, Tsuji T, 2021. Diagnosis of advanced gastric cancer using image enhancement and autofluorescence imaging systems. *Asian J Endosc Surg*, 14(4):700-706. https://doi.org/10.1111/ases.12925

Moon WK, Lin YH, O'Loughlin T, et al., 2003. Enhanced tumor detection using a folate receptor-targeted near-infrared fluorochrome conjugate. *Bioconjugate Chem*, 14(3):539-545. https://doi.org/10.1021/bc0340114

Pantalone D, Andreoli F, Fusi F, et al., 2007. Multispectral imaging autofluorescence microscopy in colonic and gastric cancer metastatic lymph nodes. *Clin Gastroenterol Hepatol*, 5(2):230-236. https://doi.org/10.1016/j.cgh.2006.11.013

Potara M, Nagy-Simon T, Focsan M, et al., 2021. Folate-targeted Pluronic-chitosan nanocapsules loaded with IR780 for near-infrared fluorescence imaging and photothermal-photodynamic therapy of ovarian cancer. *Colloids Surf B Biointerfaces*, 203:111755. https://doi.org/10.1016/j.colsurfb.2021.111755

Rawla P, Barsouk A, 2019. Epidemiology of gastric cancer: global trends, risk factors and prevention. *Gastroenterol Rev*, 14(1):26-38. https://doi.org/10.5114/pg.2018.80001

Razik NA, Al-Barakati G, Al-Heneti S, 1990. Powder diffraction data of $CdTe_xSe_{1-x}$ solid solutions. *Powder Diffract*, 5(4):206-209. https://doi.org/10.1017/S0885715600015815

Sakai H, Kawakami H, Teramura T, et al., 2021. Folate receptor α increases chemotherapy resistance through stabilizing MDM2 in cooperation with PHB2 that is overcome by MORAb-202 in gastric cancer. *Clin Transl Med*, 11(6):e454. https://doi.org/10.1002/ctm2.454

Saljoughi H, Khakbaz F, Mahani M, 2020. Synthesis of folic acid conjugated photoluminescent carbon quantum dots with ultrahigh quantum yield for targeted cancer cell fluorescence imaging. *Photodiagnosis Photodyn Ther*, 30:101687. https://doi.org/10.1016/j.pdpdt.2020.101687

Shakeri-Zadeh A, Rezaeyan A, Sarikhani A, et al., 2021. Folate receptor-targeted nanoprobes for molecular imaging of cancer: friend or foe? *Nano Today*, 39:101173. https://doi.org/10.1016/j.nantod.2021.101173

Skripka A, Mendez-Gonzalez D, Marin R, et al., 2021. Near infrared bioimaging and biosensing with semiconductor and rare-earth nanoparticles: recent developments in multifunctional nanomaterials. *Nanoscale Adv*, 3(22): 6310-6329. https://doi.org/10.1039/D1NA00502B

Songun I, Putter H, Kranenbarg EMK, et al., 2010. Surgical treatment of gastric cancer: 15-year follow-up results of the randomised nationwide Dutch D1D2 trial. *Lancet Oncol*, 11(5):439-449. https://doi.org/10.1016/S1470-2045(10)70070-X

Sung H, Ferlay J, Siegel RL, et al., 2021. Global cancer statistics 2020: GLOBOCAN estimates of incidence and mortality worldwide for 36 cancers in 185 countries. *CA Cancer J Clin*, 71(3):209-249. https://doi.org/10.3322/caac.21660

Tada K, Oda I, Yokoi C, et al., 2011. Pilot study on clinical effectiveness of autofluorescence imaging for early gastric cancer diagnosis by less experienced endoscopists. *Diagn Ther Endosc*, 2011:419136. https://doi.org/10.1155/2011/419136

Tang H, Yang ST, Yang YF, et al., 2016. Blood clearance, distribution, transformation, excretion, and toxicity of near-infrared quantum dots Ag_2Se in mice. *ACS Appl Mater Interfaces*, 8(28):17859-17869. https://doi.org/10.1021/acsami.6b05057

Tung CH, Lin YH, Moon WK, et al., 2002. A receptor-targeted near-infrared fluorescence probe for in vivo tumor imaging. *ChemBioChem*, 8(8):784-786. https://doi.org/10.1002/1439-7633(20020802)3:8<784:AID-CBIC784>3.0.CO;2-X

van Cutsem E, Sagaert X, Topal B, et al., 2016. Gastric cancer. *Lancet*, 388(10060):2654-2664. https://doi.org/10.1016/S0140-6736(16)30354-3

van Dam GM, Themelis G, Crane LMA, et al., 2011. Intraoperative tumor-specific fluorescence imaging in ovarian cancer by folate receptor-α targeting: first in-human results. *Nat Med*, 17(10):1315-1319. https://doi.org/10.1038/nm.2472

Yan HJ, You Y, Li XJ, et al., 2020. Preparation of RGD peptide/folate acid double-targeted mesoporous silica nanoparticles and its application in human breast cancer MCF-7 cells. *Front Pharmacol*, 11:898. https://doi.org/10.3389/fphar.2020.00898

Yan Y, Tian JW, Hu FR, et al., 2016. A near IR photosensitizer based on self-assembled CdSe quantum dot-aza-BODIPY conjugate coated with poly(ethylene glycol) and folic acid for concurrent fluorescence imaging and photodynamic therapy. *RSC Adv*, 6(115):113991-113996. https://doi.org/10.1039/C6RA23113F

Yang C, Bromma K, Chithrani D, 2018. Peptide mediated in vivo tumor targeting of nanoparticles through optimization in single and multilayer in vitro cell models. *Cancers*, 10(3):84. https://doi.org/10.3390/cancers10030084

Zhang Q, Deng SN, Liu JL, et al., 2019. Cancer-targeting graphene quantum dots: fluorescence quantum yields, stability, and cell selectivity. *Adv Funct Mater*, 29(5): 1805860. https://doi.org/10.1002/adfm.201805860

Supplementary information

Materials and methods